Supporting Information for

New technique to diagnose the geomagnetic field based on the

single circular current loop model

Z. J. Rong[1, 2, 3], Y. Wei[1, 2, 3], M. Yamauchi[4]，W. Y. Xu[1], D. L. Kong[5], J. Cui[6], C. Shen[7], R. X. Zhu[1, 2],

W. X. Wan[1, 2, 3], J. Zhong[1, 2, 3], L. H. Chai[1, 2, 3]

[1]Key Laboratory of Earth and Planetary Physics, Institute of Geology and Geophysics, Chinese Academy of Sciences, Beijing 100029, China

[2]College of Earth and Planetary Sciences, University of Chinese Academy of Sciences, Beijing, China

[3]Beijing National Observatory of Space Environment, Institute of Geology and Geophysics, Chinese Academy of Sciences, Beijing, China

[4]Swedish Institute of Space Physics, Kiruna, Sweden

[5]School of Atmospheric Sciences, Sun Yat-Sen University, Zhuhai 519082, China.
[6]Shanghai Astronomical Observatory, Chinese Academy of Sciences, Shanghai 200030, China

[7]Harbin Institute of Technology, Shenzhen, China,

Contents of this file

Introduction

This supplementary information contains additional details of the technique tests and the geomagnetic field dataset that we present in the paper. We provide the theoretic proof that the inverted parameters from our technique can make δ reach its extremum (Text S1). We apply the technique to the ideal circular loop field, and show that this technique is able to invert the full loop parameters exactly (Text S2, Figure S1 to S5). We compare the inversion results with the traditional least-square fitting method (Text S3). We test the

technique when the magnetic source is current flowing on a spherical surface (Text S4, Table S1). Table S2 lists the geomagnetic field dataset used in Section 4.

Text S1.

The mathematical proof of the extremum of δ

The dimensionless error δ defined in Eq. (17) of body text is, in principle, the function of the full loop parameters $\{ x_0^{'}, y_0^{'}, z_0^{'}, \theta_0, \varphi_0, a, I \}$. Here, we show that, the derived loop parameters $\{ x_{0m}^{'}, y_{0m}^{'}, z_{0m}^{'}, \theta_{0m}, \varphi_{0m}, a_m, I_m \}$ from our technique indeed make δ reach its extremum.

Because α in Eq.(3) is the function of $\{ x_0^{'}, y_0^{'}, \theta_0, \varphi_0 \}$, $\alpha_{\min}$ is the function of $\{ \theta_0, \varphi_0 \}$, and ε in Eq.(15) is the function of $\{ z_0^{'}, a \}$, δ is actually the function of $\{ \sigma, \varepsilon, I \}$. The extremum of δ is reached when all the partial differential solutions of δ equal zero. Obviously, when $x_0^{'} = x_{0m}^{'}$, $y_0^{'} = y_{0m}^{'}$, we have $\dfrac{\partial \delta}{\partial x_0^{'}} = \dfrac{\partial \delta}{\partial \alpha} \dfrac{\partial \alpha}{\partial x_0^{'}} = 0$ and $\dfrac{\partial \delta}{\partial y_0^{'}} = \dfrac{\partial \delta}{\partial \alpha} \dfrac{\partial \alpha}{\partial y_0^{'}} = 0$.

Similarly,   when $x_0^{'} = x_{0m}^{'}$, $y_0^{'} = y_{0m}^{'}$, $\theta_0 = \theta_{0m}$, $\varphi_0 = \varphi_{0m}$,   we   have $\dfrac{\partial \delta}{\partial \theta_0} = \dfrac{\partial \delta}{\partial \alpha} \dfrac{\partial \alpha}{\partial \alpha_{\min}} \dfrac{\partial \alpha_{\min}}{\partial \theta_0} = 0$, and $\dfrac{\partial \delta}{\partial \varphi_0} = \dfrac{\partial \delta}{\partial \alpha} \dfrac{\partial \alpha}{\partial \alpha_{\min}} \dfrac{\partial \alpha_{\min}}{\partial \varphi_0} = 0$ .In the same way, when $x_0^{'} = x_{0m}^{'}$, $y_0^{'} = y_{0m}^{'}$, $\theta_0 = \theta_{0m}, \varphi_0 = \varphi_{0m}, z_0^{'} = z_{0m}^{'}$, $a = a_m$,   we have $\dfrac{\partial \delta}{\partial z_0^{'}} = \dfrac{\partial \delta}{\partial \varepsilon} \dfrac{\partial \varepsilon}{\partial z_0^{'}} = 0$ and $\dfrac{\partial \delta}{\partial a} = \dfrac{\partial \delta}{\partial \varepsilon} \dfrac{\partial \varepsilon}{\partial a} = 0$. Finally, when $x_0^{'} = x_{0m}^{'}$, $y_0^{'} = y_{0m}^{'}$, $\theta_0 = \theta_{0m}, \varphi_0 = \varphi_{0m}, z_0^{'} = z_{0m}^{'}$, $a = a_m$, $I = I_m$, we have $\dfrac{\partial \delta}{\partial I} = 0$.

In other words, the loop parameters $\{ x_{0m}^{'}, y_{0m}^{'}, z_{0m}^{'}, \theta_{0m}, \varphi_{0m}, a_m, I_m \}$ from our technique can make all the partial differential solutions of δ equal zero, and δ must reach its extremum with the derived loop parameters.

Text S2.

Inversion with magnetic source of single loop

To test the validity of this technique, we construct a circular current loop model with given parameters to generate the loop field which is sampled by a virtual spacecraft along

an arbitrary trajectory. If the algorithm of technique is valid, the application to the sampled dataset should be able to invert the loop parameters exactly.

The input loop parameters are like this: the location of loop center is at $\mathbf{r}_0$ ($x_0=0.1$, $y_0=0.2$, $z_0=0.5$) m, the loop radius is $a=0.5$m, the carried electric current is $I=0.35$A, and the loop axis orientation is $\hat{\mathbf{M}}$ ($\theta_0=60°$, $\varphi_0=40°$).

Using these loop parameters, the sampled magnetic field data can be analytically computed via Eqs. (8-12). The test here is to apply our technique with the sampled magnetic field to invert the input parameters $\mathbf{r}_0$, a, I, and $\hat{\mathbf{M}}$.

The spacecraft's trajectory is arbitrarily assumed to be linearly varied from (x= -2, y= -2, z= -2) m to (x=2, y=2, z=2) m, and spacecraft evenly records the magnetic field with, arbitrarily, 20 data points. The time series of the sampled magnetic field are shown in Figure S1.

Using Eqs. (2)-(7), we calculate α_{min} for all possible orientations of $\hat{\mathbf{M}}$ (θ_0, φ_0). In Figure S2, we show the 2-D distribution of α_{min} in the map constituted by θ_0 and φ_0. Obviously, as expected, there are two global minima of α_{min} present in Figure S2. One is about at ($\theta_0=60°$, $\varphi_0=45°$), the other one is about at ($\theta_0=120°$, $\varphi_0=225°$). The two minima should correspond to the parallel and anti-parallel direction of $\hat{\mathbf{M}}$. With the reading of the initial values of θ_0 and φ_0 around the two minima, the two optimum candidate directions of $\hat{\mathbf{M}}$, $\hat{\mathbf{M}}_1$ and $\hat{\mathbf{M}}_2$, as well as the corresponding loop centers ($x_0^{'}$, $y_0^{'}$) are derived. The yielded $\hat{\mathbf{M}}_1$ is ($\theta_0=60°$, $\varphi_0=40°$), and $\hat{\mathbf{M}}_2$ is ($\theta_0=120°$, $\varphi_0=220°$), and both of them are nearly anti-parallel to each other.

To determine which one is the final direction of $\hat{\mathbf{M}}$, in Figure S3, we show the projection of magnetic field vectors on the equatorial plane, i.e. $\mathbf{b}_{ip}$, according to the two candidate axis directions. In Figure S3, the projections are only shown when spacecraft is at the hemisphere $\hat{\mathbf{M}}$ pointing away ($z_i^{'} > 0$, or $\mathbf{r}_i \cdot \hat{\mathbf{M}} > 0$). It is clear that, in this hemisphere, the magnetic field vectors basically point radially outward along $\hat{\mathbf{M}}_1$ (see Figure S3a, one inward magnetic vector is actually induced by the axis shift of the loop center), but inward along $\hat{\mathbf{M}}_2$ (see Figure S3b). Thus, we choose $\hat{\mathbf{M}}_1$ as the final

optimum direction of $\hat{\mathbf{M}}$, that is $\hat{\mathbf{M}}$ (θ_0=60°, φ_0=40°). Accordingly, the components of loop center via Eq. (7) are calculated as $x_0^{'}$ = -0.2455 m and $y_0^{'}$ = -0.2383 m.

Further, as shown in Figure S4, with the derived $\hat{\mathbf{M}}$, $x_0^{'}$ and $y_0^{'}$, the distribution of ε can be plotted as a function of $z_0^{'}$ and a via Eq.(15). Consequently, with the initial optimum value of $z_0^{'}$ and a from Figure S4 ($z_0^{'}$ = a =0.5 m) , the optimum value of $z_0^{'}$ and a, corresponding to the global minimum of ε, is found to be $z_0^{'}$ =0.4277 m, and a=0.5 m, respectively.

Finally, with the derived $\hat{\mathbf{M}}$, $x_0^{'}, y_0^{'}, z_0^{'}$ and a, we calculate δ via Eq. (17) with varied current I, and plot the variation of δ against I in Figure S5. The numerical calculation demonstrates that δ reaches its minimum when I=0.35 A via Eq. (17).

Using Eq. (1), the transformation of the loop center $\mathbf{r}_0$ ($x_0^{'}$=-0.2455, $y_0^{'}$=-0.2383, $z_0^{'}$ =0.4277) m in the loop coordinates into the Cartesian coordinates yields $\mathbf{r}_0$ = (x_0=0.1, y_0=0.2, z_0=0.5) m. Considering the inverted $\hat{\mathbf{M}}$ (θ_0=60°, φ_0=40°), a=0.5 m, and I=0.35 A, obviously, our technique can exactly invert the full parameters of a circular current loop model if the sampled magnetic field is the ideal loop field.

Text S3.

Comparison with the non-linear fitting method

In the "Introduction" of text body, we state that all the past methods employed the least-square fitting methods to fit the loop parameters simultaneously. Here, with the same sampled field dataset in **Text S2**, we show the comparison of our technique with the fitting method.

The three Cartesian components of the sampled magnetic field vectors are denoted as B_{ix}, B_{iy}, and B_{iz}. While, the field components predicted by the loop model are B_{iX}, B_{iY}, and B_{iZ}, which are the functions of the loop parameters $\mathbf{r}_0$, a, I, and $\hat{\mathbf{M}}$. B_{iX}, B_{iY}, and B_{iZ} can be calculated via Eqs.(8-12). We can construct a least-square residual error as

$$Res\left(\mathbf{r}_0, a, I, \mathbf{M}\right) = \sum_i \left[\frac{\left(B_{ix} - B_{iX}\right)^2 + \left(B_{iy} - B_{iY}\right)^2 + \left(B_{iz} - B_{iZ}\right)^2}{B_{ix}^2 + B_{iy}^2 + B_{iz}^2} \right]^{1/2}$$

The optimum parameters should make the residual error, *Res*, reach the minimum, which could be solved by the function demand "**fminsearch**" of **Matlab.**

As expected, the yielded fitting parameters is indeed strongly dependent on the initial input parameters we chosen. If the initial parameter set is not far from the real parameters, for example, chosen as $\{\mathbf{r}_0$ (x_0=0.08, y_0=0.1, z_0=0.4) m; a=0.4m; I=0.3A; **M**= (θ_0=65°, φ_0=45°)$\}$, then the real parameters can be well fitted by the optimization, that is$\{\mathbf{r}_0$ = (x_0=0.1, y_0=0.2, z_0=0.5) m; a=0.5m; I=0.35A; **M** (θ_0=60°, φ_0=40°)$\}$.

In contrast, if the initial parameters are set as $\{\mathbf{r}_0$ (x_0=0, y_0=0, z_0=0) m; a=0.5m; I=0.35A; **M** (θ_0=60°, φ_0=40°)$\}$, then the output shows that optimization calculation quits due to exceeding the iteration times, and the returned parameters yields $\{\mathbf{r}_0$ (x_0=0.14, y_0=0.40, z_0=0.08) m; a=0.61m; I=0.21A; **M** (θ_0=61.99°, φ_0=46.33°)$\}$.

Obviously, in comparison with the least-square fitting, our technique can effectively avoid the dilemma of setting initial values.

Text S4.

Inversion with magnetic source of current on a spherical surface

Although our technique works well for the ideal loop currents, it is still unknown whether it works well for the other more complicated current patterns. To test the technique ability for the complicated currents pattern, the pattern of dynamo current could be more plausible seen as the current flowing on a spherical surface instead of the loop current.

According to the Biot-Savart law, the magnetic field generated by the current flowing on a spherical surface can be calculated as

$$\mathbf{B}(x,y,z) = \frac{\mu_0}{4\pi} \iint \frac{j d\mathbf{s} \times \mathbf{R}}{R^3}$$

Where, j is the surface current density, and **R** is the displacement vector to the spherical center.

Here, to simplify the calculation, we assume that j is only dependent on the polar angle (colatitude), and considered the cases when $j= j_0*cos^2\theta$, $j_0*(cos^2\theta)^{1/2}$, j_0, $j_0*sin\theta$, $j_0*sin^2\theta$, $j_0*sin^5\theta$, $j_0*sin^{10}\theta$, $j_0*sin^{20}\theta$, and $j_0*sin^{50}\theta$, respectively.

As shown in Figure S6, in a given Cartesian coordinate, the input parameters are arbitrarily specified, that is, $\mathbf{r}_0$ =(x_0=0, y_0=0.2, z_0=0.3) m, a=0.5 m, j_0=0.2 Am^{-2}, and $\hat{\mathbf{M}}$ = (θ_0=45°, φ_0=150°).To make the sampled data evenly, four polar circular orbits with radius being 1 m are constructed. The longitude coverage of the four orbits are the same as that studied in Section 3.1. Along each orbit, 20 data points are sampled. In total, 80 field vectors are obtained from the four orbits.

After performing our technique for the different cases of surface current density distributions, the yielded loop parameters are tabulated correspondingly in Table S1.

It is clear from Table S1 that the loop model can well recover the displacement of sphere center and the magnetic axis orientation if the surface currents are flowing purely azimuthally. Interestingly to note that, for the cases of $j= j_0*cos^2\theta$, $j_0*(cos^2\theta)^{1/2}$, j_0 and $j_0*sin\theta$, the optimum loop radius cannot be find, and the inversion calculation is aborted. The failure of inversion in these cases is understandable, because the external field of $j= j_0*sin\theta$ is the ideal dipole field whose loop radius is zero (see http://photonics101.com/magnetostatic-fields-in-matter/surface-current-on-sphere). As j increases with the latitude, e.g. $j= j_0$, $j_0*(cos^2\theta)^{1/2}$, $j_0*cos^2\theta$, the induced external fields are more elongated than the dipole field along magnetic axis orientation, thus the optimum loop radius cannot be inverted also.

In contrast, as j becomes concentrated more than $j_0*sin\theta$ towards magnetic equatorial plane, e.g. $j= j_0*sin^2\theta$, $j_0*sin^5\theta$, $j_0*sin^{10}\theta$, $j_0*sin^{20}\theta$, and $j_0*sin^{50}\theta$, our inversion calculation can be performed successfully. The inversion results demonstrate that: 1. the equivalent loop radius is smaller than the real spherical radius; 2. the loop radius is approaching the real spherical radius as j concentrates more in magnetic equatorial plane.
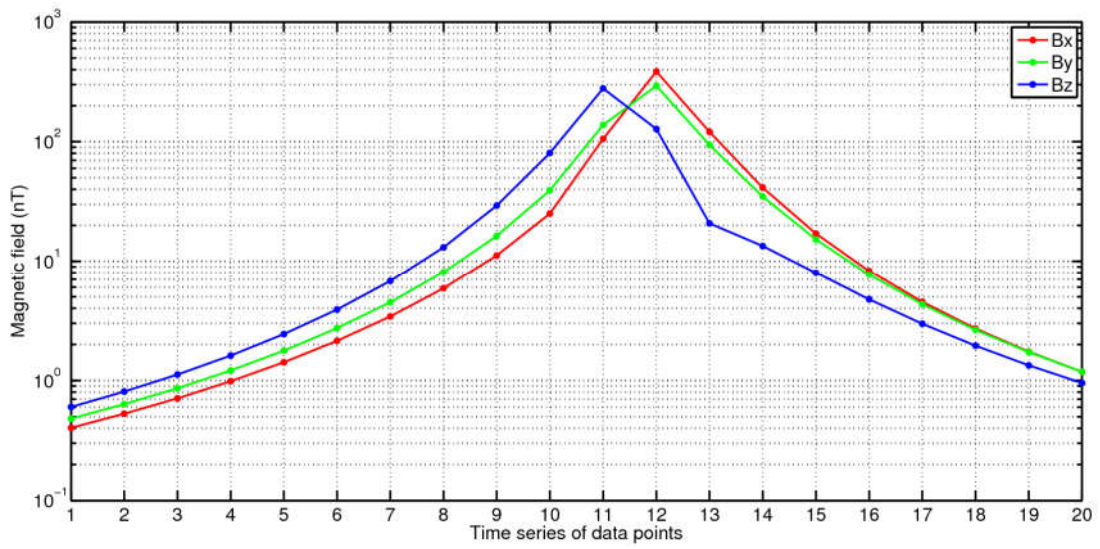
Figure S1. The time series of magnetic field along spacecraft's trajectory.
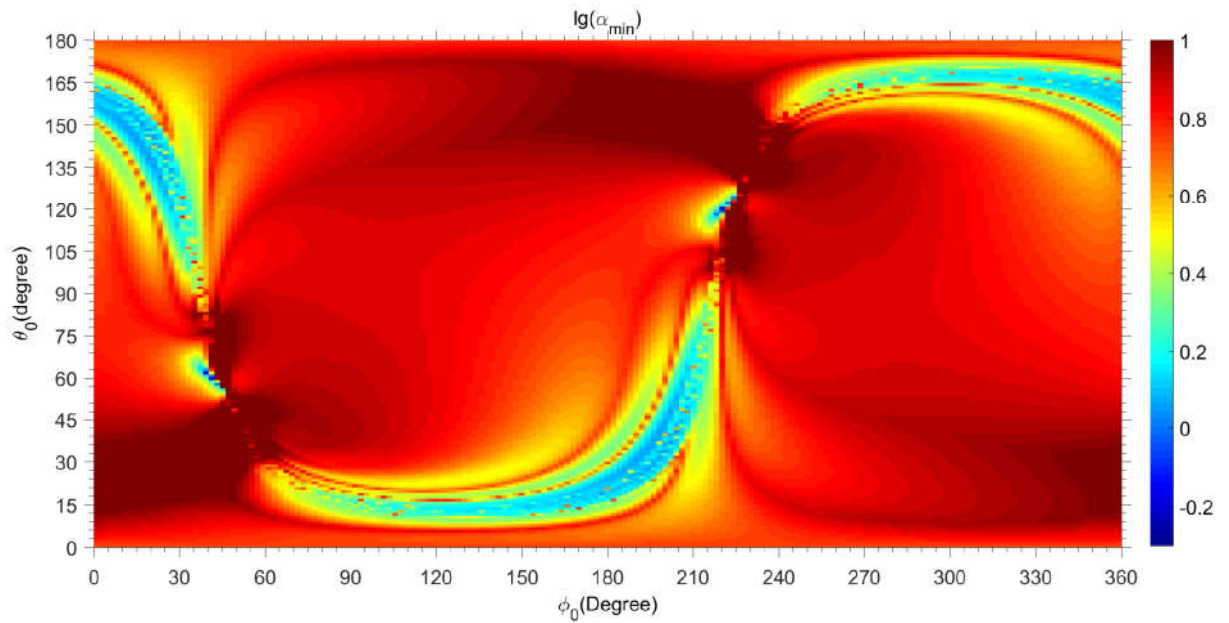
Figure S2. The distribution of α_{min}. To identify the global minimum easily, we show the distribution of $\lg(\alpha_{min})$ in this plot.
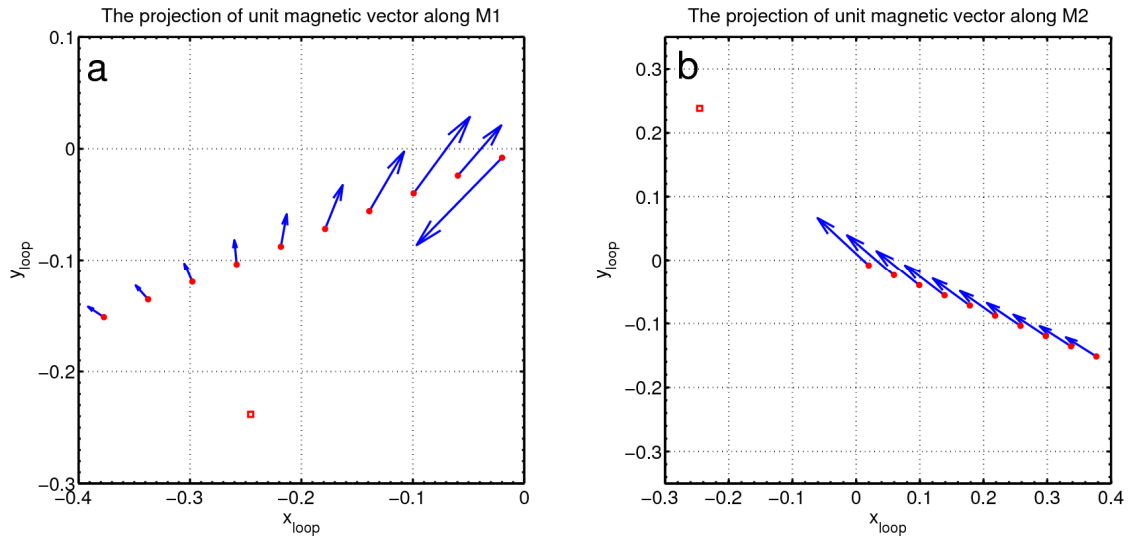
Figure S3. The projection of magnetic field direction on the equatorial plane of loop coordinates. The red dots represent the location of spacecraft with $z_i' > 0$, the blue arrows are the projected directions of sampled field vectors, and the red square represents the loop center.
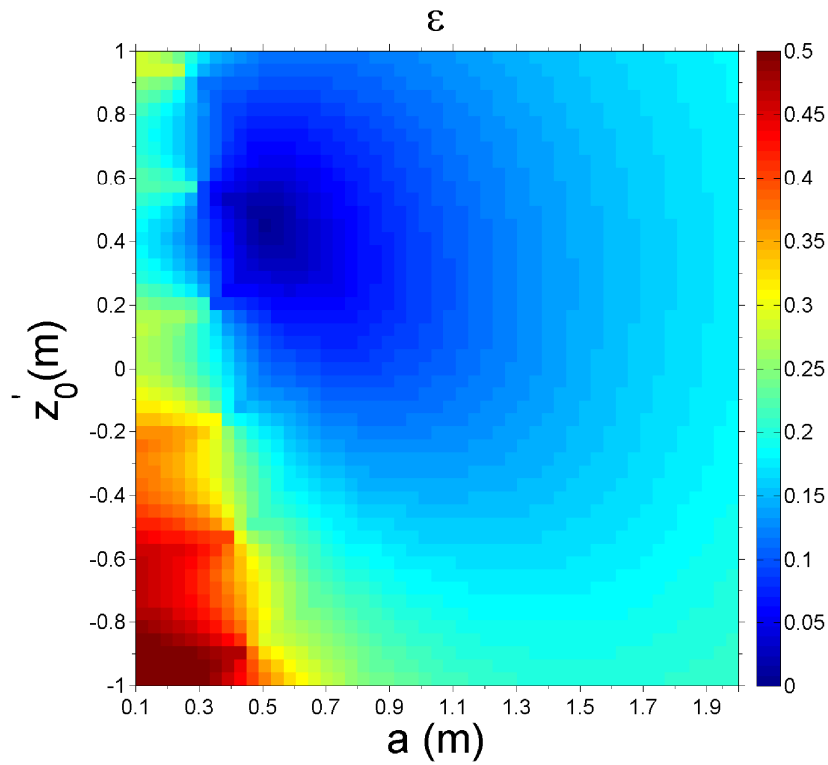
Figure S4. The 2-D distribution of ε
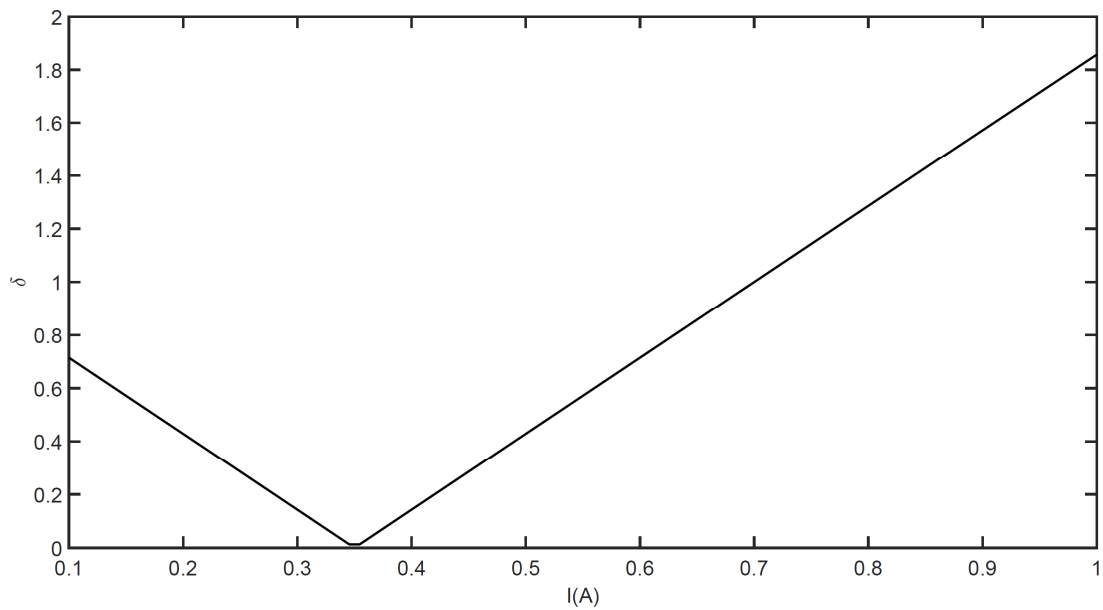
Figure S5. The variation of δ against I.
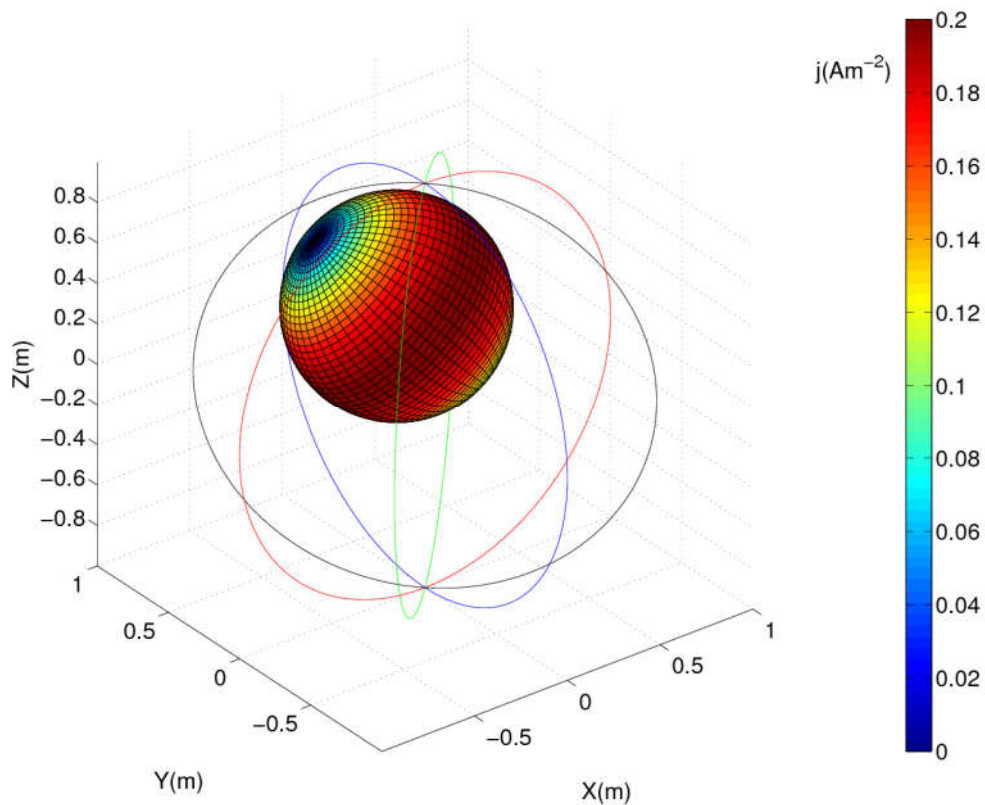
Figure S6. Test with four orbits on the magnetic field whose source is the current on a spherical surface. The distribution of surface current density j=0.2*$sin\theta$ is colored.

Table S1. The inversed single loop parameters when magnetic source is the current flowing on a spherical surface.

| Models	x_0 (m)	y_0 (m)	z_0 (m)	a (m)	I (A)	M (Am2)	θ_0 (°)	φ_0 (°)	α_{min} (°)	ε (°)	δ
$j_0*cos^2\theta$	~	~	~	~	~	~	45	150	0	~	~
$j_0*(cos^2\theta)^{1/2}$	~	~	~	~	~	~	45	150	0	~	~
j_0	~	~	~	~	~	~	45	150	0	~	~
$j_0*sin\theta$	~	~	~	~	~	~	45	150	0	~	~
$j_0*sin^2\theta$	-0.0002	0.2001	0.3002	0.1980	0.7522	0.0926	45	150	0	0.1310	0.0040
$j_0*sin^5\theta$	-0.0004	0.2003	0.3005	0.3245	0.2177	0.0720	45	150	0	0.3438	0.0101
$j_0*sin^{10}\theta$	-0.0006	0.2003	0.3006	0.3919	0.1157	0.0558	45	150	0	0.4229	0.0123
$j_0*sin^{20}\theta$	-0.0004	0.2002	0.3005	0.4389	0.0687	0.0416	45	150	0	0.3741	0.0111
$j_0*sin^{50}\theta$	-0.0002	0.2001	0.3002	0.4743	0.0385	0.0272	45	150	0	0.2290	0.0069

Table S2. The geomagnetic field data of global geomagnetic observatories recorded on 2015-01-01 00:00:00. The columns from left to the right show the IAGA name of observatories, the latitude and longitude of observatories, the northward (X), the eastward (Y), the downward (Z) component, and the field strength (F) of geomagnetic field in the local geographic coordinates, respectively. The unavailable data is assigned as 99999. The field data can be also accessible at the website http://www.intermagnet.org/index-eng.php

IAGA code	Latitude(Deg.)	Longitude(Deg.)	X(nT)	Y(nT)	Z(nT)	F(nT)
AAA	43.2	73.9	24668.5	2177.4	49102.2	54993.05
AAE	9.03	38.7	36252.54	1240.1	1954.29	36326.32
ABG	18.62	72.87	38119.1	140.1	19810.8	42960
ABK	68.358	18.823	11335.7	1617.8	51892.1	53140.63
AIA	-65.25	295.75	19954.7	5694.2	-32135.8	99999
AMS	-37.8	77.57	13805.42	-11710	-49494.34	52697.46
API	-13.8	188.22	32655	6915.6	-20051	38938.23
ARS	56.433	58.567	15650.6	3709.3	53880.1	56229.18
ASC	-7.95	345.62	19931.6	-5472	-19684.1	28542.21
ASP	-23.77	133.88	30086	2477.8	-43767.5	53168.61
BDV	49.08	14.02	20382.5	1201.2	44139.2	48632.69
BEL	51.84	20.79	18922.5	1902.3	46474.3	50214.84
BFO	48.331	8.325	20943.6	677.3	43306.1	48109.37
BLC	64.318	263.988	6707	-369.4	58424.6	58809.48
BMT	40.3	116.2	28024.1	-3868.1	47270.5	55088.83
BOU	40.14	254.76	20550.2	3183.4	48047.5	52354.62
BOX	58.07	38.23	15257.3	3235.8	50272	52635.92
BRD	49.87	260.0261	15038.3	1420.3	55142	57173.39

BRW	71.34	203.38	8704	2444.3	56745.3	57460.77
BSL	30.35	270.36	23936.6	-325	41303.7	47739.52
CKI	12.1875	96.8336	34568.1	-1405.4	-32752	47640.55
CLF	48.02	2.27	21182.9	61.6	42863.4	47812.03
CMO	64.87	212.14	11883.6	4023.5	55425.9	56827.95
CNB	35.32	149.36	23179.3	5135	-52954.3	58032.5
CSY	66.283	110.533	-979.1	-9134.7	-63394.6	64056.32
CTA	-20.1	146.3	31501.2	4092.2	-37470.4	49123.04
CYG	36.37	126.854	30083.6	-4088.4	40104.3	50299.93
CZT	-46.43	51.87	10455.1	-12388.9	-34451.3	38074.95
DED	70.36	211.21	8438.4	2931.1	56861.7	57558.41
DLT	11.94	108.48	40778.7	-458	8164.1	41590.64
DMC	-75.25	124.167	-8247.96	-6407.33	-61822.25	62702.75
DOU	50.1	4.6	20103.6	261.4	44184.9	99999
DRV	-66.67	140.01	-1868.96	169.21	-69110.94	69140.11
EBR	40.957	0.333	25189.8	18.7	37497.7	45173.14
ESK	55.32	356.8	17512.3	-834.1	46449.5	49648.29
EYR	-43.474	172.393	99999	99999	99999	99999
FCC	58.759	265.912	9400.2	-286.9	57838.6	58598.11
FRD	38.2	282.63	21012	-3920.5	46700.2	51359.35
FRN	37.09	240.28	22772.5	5304.4	42388.9	48410.14
FUR	48.17	11.28	20951.4	982.2	43458.2	48254.66
GAN	0.6946	73.1537	37647.7	-2856.2	-13130.3	39974.49
GCK	44.6	20.8	22677.8	1713.6	42039.3	47796.87
GDH	69.252	306.467	7400.4	-4996.1	55745.6	99999
GNG	-31.356	115.715	23945.2	-712.1	-52701.6	57891.34
GUA	13.59	144.87	35784.3	687.9	7943.1	36661.62
GUI	28.32	343.57	27540.5	-3705	22732	35901.85
HAD	51	355.52	19709.7	-817	44330.4	48521.48
HBK	-25.88	27.71	12360.2	-3997.4	-25171.8	28325.29
HER	-34.43	19.23	9569.2	-4581.8	-23325.3	25624.83
HLP	54.61	18.82	17505.7	1436.1	47141.7	50306.77
HON	21.32	202	26997.3	4645.8	21217	34649.66
HRB	47.86	18.19	20986.3	1554.2	43795.2	99999
HRN	77	15.37	7821.1	1002.5	53989.7	99999
HUA	-12.05	284.67	24974.2	-1143.6	-106	99999
HYB	17.4	78.6	39421.5	-516.9	17637.6	43190.25
IPM	-27.2	250.58	25046.2	7052.7	-19454.9	32489.57
IQA	63.753	291.482	8260.1	-4241.1	56300	57060.45
IRT	52.27	104.45	18554.6	-1127.4	57411.9	99999
IZN	40.5	29.72	25063.1	2232.3	40205.6	47430.39
JAI	26.92	75.8	35233.2	35.6	31190.1	99999
JCO	70.356	211.201	8451.4	2954.2	56862	57561.79
KAK	36.23	140.18	29709.5	-3827.8	35694.1	46598.02
KDU	-12.69	132.47	35421.7	1972.5	-29611.6	46210.76
KEP	-54.282	323.5071	15630.5	-1968.4	-23076.7	27941.29

KHB	47.61	134.69	23334	-5251.5	49170.3	99999
KIV	50.72	30.3	19170.7	2545.9	46676.3	99999
KMH	-26.54	18.11	99999	99999	99999	99999
KNY	31.42	130.88	32475.8	-3662	33146.3	46548.52
KOU	5.21	307.27	26564.8	-8593.8	7606.4	28937.75
LER	60.13	358.82	15018.5	-505.9	48610.8	50880.46
LON	45.4081	16.6592	22343.9	1460.8	42199.7	99999
LRM	-22.22	114.1	30128	156.4	-43457.9	52879.75
LVV	49.9	23.75	19907.8	2113.1	45628	99999
LYC	64.6	18.8	13016.5	1539.8	50573.1	52243.93
LZH	36.1	103.84	30550.9	-1228.2	43962.5	53549.87
MAB	50.298	5.682	19972.2	377	44444.2	99999
MAW	-67.6	62.88	6918.8	-17189.4	-45572.9	49196.27
MBO	14.38	343.03	32193.1	-4218.1	4072.6	32722.88
MCQ	-54.5	158.95	10756	6701.9	-62844.8	64109.48
MEA	54.616	246.653	13509.2	3607.2	55739.9	57466.92
MGD	60.051	150.728	16797.6	-3995.4	53468	56186.54
MMB	43.91	144.19	25801.7	-4016.1	42401.5	49797.03
NAQ	61.16	314.558	11844.1	-5087.9	52878.4	99999
NCK	47.63	16.72	21120	1448.5	43529.3	99999
NEW	48.27	242.88	17465.2	4788	51731.1	54809.35
NGK	52.07	12.68	18853	1054	45560.5	49318.41
NUR	60.51	24.66	14815.3	2054.7	50050.1	99999
NVS	54.85	83.23	16208	2358.1	57418.5	59709.03
ORC	-60.737	315.26	17817.8	-304.27	-26857.2	32484.9
OTT	45.4003	284.448	17703.2	-4353.3	51384.4	54522.88
PAF	-49.35	70.26	10094.95	-14707.92	-45849.94	49198.65
PAG	42.5	24.2	23692.8	1804.8	40799	47213.83
PEG	38.1	23.9	26416	1987.4	37500.8	45916.1
PET	52.971	158.248	21491.9	-2282.2	47153.5	51870.84
PHU	21.03	105.95	38825	-960.7	23103.6	45189.48
PPT	-17.57	210.42	29268.5	5877.5	-19094.9	35436.95
PST	-51.7	302.11	18341.3	964.2	-21702	28430.79
RES	74.69	265.105	2409.2	-1079.3	57614.3	57674.65
SBA	-77.85	166.78	99999	99999	99999	99999
SBL	43.9321	299.9905	19745.5	-6350.9	46362	50789.99
SFS	36.667	354.055	27509.3	-801.5	33020.9	42985.86
SHU	55.35	199.54	19407.8	3928.3	48428	52320.24
SIT	57.06	224.67	14876.5	5275	53497	55776.82
SJG	18.11	293.85	26302.6	-5978.9	25642.4	37217.12
SOD	67.37	26.63	11302.4	2255.5	51560.7	52833.21
SON	25.1168	66.4487	34794.98	419.15	27940.2	44626.3
SPG	60.542	29.716	14542.3	2548.3	50257	52381.11
SPT	39.55	355.65	25994.4	-560.7	35894.6	44322.17
STJ	47.595	307.323	18799.1	-6286.3	47138.2	51136.42
SUA	44.68	26.25	22590.4	2086.4	42662.6	48319.23

TAM	22.79	5.53	33686.3	6.7	17095.3	37775.97
TDC	-37.067	347.685	9461.3	-3793.6	-22426.8	24635.01
THL	77.47	290.773	2734.2	-3087.2	56189.7	99999
THY	46.9	17.89	21495.1	1533.4	43213.1	48288.33
TRW	-43.3	294.7	19655.84	1734.3	-17790.3	26567.7
TSU	-19.202	17.584	14052.7	-2288.8	-25835.5	99999
TUC	32.18	249.27	24052.2	3988.2	40782.5	47514.29
UPS	59.903	17.353	15130.4	1430	49050.8	51351.29
VAL	51.933	349.75	19379.5	-1664.3	44733.1	99999
VIC	48.52	236.58	18081.6	5374.9	50457.8	53867.68
VNA	-70.683	351.718	99999	99999	99999	99999
VOS	-78.464	106.835	-7519.2	-11337.8	-57798	99999
VSS	-22.4	316.35	16896.58	-6989.06	-14428.1	23290.67
WIC	47.9305	15.8657	20989.4	1377	43659.1	48461.93
WNG	53.74	9.07	18158	713.1	46133.6	49583.27
YAK	61.96	129.66	13457	-4944.6	58145.1	59882.7
YKC	62.48	245.518	8800.7	2715.9	57798.2	58527.63